COMPARATIVE SPECTROSCOPIC STUDY OF THE Dy^{3+} DOPED DOUBLE CHLORIDE AND DOUBLE FLUORIDE CRYSTALS FOR TELECOMMUNICATION AMPLIFIERS AND IR LASERS*

A. TKACHUK[a†], S. IVANOVA[b], L. ISAENKO[c], A. YELISSEYEV[c], STEVE PAYNE[d], R. SOLARZ[d], M. NOSTRAND[d], R. PAGE[d] AND STEPHEN PAYNE[d]

[a]S.I. Vavilov State Optical Institute, St. Petersburg, Birzhevaya line, 12, 199034, Russia
[b]St. Petersburg State University, Department of Physics, Petrodvoretz, 198904, Russia
[c]Design and Technological Institute for Monocrystals SB RAS
Russkaya str. 43, Novosibirsk, 630058, Russia
[d]Lawrence Livermore National Laboratory, CA, L-590
P.O. Box 5508, Livermore, California 94550, USA

(Received July 23, 1998; revised version January 20, 1999)

In this work we studied spectroscopic characteristics of potassium-lead double-chloride, and lithium-yttrium double-fluoride crystals doped with dysprosium. Objects of research were $KPb_2Cl_5:Dy^{3+}$, and $LiYF_4(YLF):Dy^{3+}$ crystals grown by the Bridgman–Stockbarger technique. We obtained the effective distribution coefficients $K_{Dy} = 0.95$ for $LiYF_4:Dy^{3+}$, and $K_{Dy} = 1$ for $KPb_2Cl_5:Dy^{3+}$. Optical spectra were studied, intensity parameters were determined by the Judd–Ofelt method, and radiative probabilities and branching ratio were calculated. The conclusion was made that the studied crystals can be considered as promising new active media for laser diode pumped solid state lasers. The $YLF:Dy^{3+}$ crystals are perspective for laser action near 3 mm, and the $KPb_2Cl_5:Dy^{3+}$ for multiwavelength IR lasers, and for 1.3 mm laser diode pumped telecommunication amplifiers.

PACS numbers: 78.55.–m

1. Introduction

Development of the Er-doped amplifiers (EDFAs) for telecommunications gave rise to increasing rates of data transmission, however, it should be noted that the EDFA operates at 1.55 μm which differs from 1.31 μm operating wavelength

*The results of this paper were initially presented at *The Jabłoński Centennial Conference on Luminescence and Photophysics, July 23–27, 1998, Toruń, Poland.*

†e-mail: alex@tkachuk.spb.su

format. That is why a problem of creating the amplifiers operating at 1.31 μm remains actual.

The rare-earth doped fluoride crystals are well known as luminescent and laser material with laser emission in the UV, VIS, and IR including the 1.3 μm spectral region. YLF-crystalline matrix shows a wide transparency range (from 0.15 to 7.5 μm), it has the best thermooptical characteristics, low value of induced nonlinear refractive index, and optical, thermal, and radiation stability. Dysprosium doped fluoride crystals BaY_2F_2:Dy^{3+}, Er^{3+} [1] and LaF_3:Dy^{3+} [2] are known as active media for IR solid state lasers emitting at 3 μm.

The narrower phonon spectrum of chloride crystals in comparison with the fluoride makes the chlorides one of the best materials for laser action in the middle IR spectral region where luminescence of fluoride crystals is quenched by fast multiphonon relaxation. An attempt was made for searching a new crystalline matrix in which laser action could be obtained under LD pumping in a wide spectral region including the wavelength near 1.3 μm which is favorable for optical telecommunication amplifiers.

The knowledge of the radiative probabilities of the transitions in rare-earth ions is useful for prediction of its possible laser applications, for this reason we tried to compare the spectroscopic parameters of Dy^{3+}-doped crystals of double chlorides with well-known YLF laser matrix.

We studied optical spectra of double-chloride KPb_2Cl_5:Dy^{3+} and double-fluoride YLF:Dy^{3+} crystals grown by Bridgman technique. We obtained the effective distribution coefficients of Dy^{3+} in fluoride and chloride crystals: $K_{Dy} = 0.95$ and $K_{Dy} = 1$ for the YLF:Dy^{3+} and KPb_2Cl_5:Dy^{3+}, respectively. The ESR measurements revealed the only type of impurity centers in each of studied systems. The absorption and luminescence spectra were studied, the intensity parameters were determined by the Judd–Ofelt method, and the radiative and non-radiative transition probabilities were calculated for Dy^{3+}-doped double chloride and double fluoride crystals.

2. Experimental methods and results

2.1. Crystal growth and structure

KPb_2Cl_5:Dy^{3+} crystals were grown by Bridgman technique from the ampoule in a double-zone furnace with vertical gradient 20 deg/cm. The KPb_2Cl_5 crystals have monoclinic structure with lattice constants $a = 0.8831$ nm, $b = 0.7886$ nm, $c = 1.2430$ nm and angles $\alpha = \gamma = 90°$, $\beta = 90°8'$; space symmetry group P_21/c. It was found that in KPb_2Cl_5 there are four non-equivalent sites of Pb^{2+}, so there are different possibilities for replacement the cations (Pb^{2+} and K^+) by Dy^{3+}. The charge compensation with forming the cation vacancy is required in Dy^{3+} doped chloride crystals. The Dy content in the melt did not exceed 3 mol.%. The samples were polished disks 6 mm in diameter and thickness of 1–8 mm. The concentration of the Dy^{3+} ions in a melt varied from 0.5 to 2 at.%.

YLF:Dy^{3+} crystals were grown from carbon crucibles by the modified high vacuum Stockbarger technique from the stoichiometric fusion mixture. YLF-crystals are uniaxial, positive, have scheelite structure with lattice parameters $a =$

0.5175 nm and $c = 1.074$ nm. Space symmetry group of YLF crystals is C_{4h}, point symmetry group at the Y^{3+} site is S_4. Dy^{3+} substitution occurs at the Y^{3+} site, and charge compensation is not required. The samples were polished cuboids with the dimensions $6 \times 6 \times 6$ mm^3 and crystallographic "c"-axis oriented along one of the ribs. Dy^{3+} concentration in the YLF samples up to 100 at.% was achieved, scheelite structure of the $LiDyF_4$ crystals was confirmed by X-ray method.

2.2. Determination of the distribution coefficient of Dy^{3+} ions in crystals

Since the distribution coefficients of dysprosium in KPb_2Cl_5 and YLF matrices were unknown, a simple non-destructive spectrophotometric method of determination of average dysprosium concentration in the sample was developed. We determined the effective distribution (segregation) coefficient K_{Dy} using the method based on the measuring of the peak optical density D_λ in the reference line at the wavelength λ and on the known peak absorption cross-section $\sigma_a(\lambda)$, similarly to the method described in [3]. The average dysprosium concentration N_{Dy} in sample of length L was defined from the expression

$$N_{Dy}[\mathrm{cm}^{-3}] = 2.3D(L[\mathrm{cm}] \cdot \sigma_a(\lambda)[\mathrm{cm}^2])^{-1}. \tag{2.1}$$

The calibration of the absorption method was carried out using reference crystal sample with the known concentration of dysprosium. Dy^{3+} concentration in this reference sample was determined by the X-ray spectral analysis performed with the electron-probing micro-analyzer Camebax by CAMEKA. The samples were cut from different parts of the boule and prepared in the form of thin polished plates. The YLF:Dy^{3+} samples were oriented with the crystallographic axis "c" normally to the face to avoid the polarization dependence of $\sigma_a(\lambda)$. The absorption spectra of these samples were recorded with a Perkin-Elmer Lambda-9 spectrophotometer and the peak absorption cross-sections $\sigma_a(\lambda)$ were determined for each of the samples.

Our measurements showed that the segregation coefficient K_{Dy} for KPb_2Cl_5:Dy^{3+} was equal to 1.003, and K_{Dy} for YLF:Dy^{3+} crystals was close to unity, namely, $K_{Dy} = 0.95$. This value did not change along the crystal length up to 50 mm with the accuracy about 0.2%.

2.3. Optical spectra and spectroscopic parameters

We investigated the optical spectra of the KPb_2Cl_5:Dy^{3+} and YLF:Dy^{3+} crystals by traditional spectroscopic methods. The energy scheme of Dy^{3+} ions is shown in Fig. 1. The ground state absorption, most probable emission and non-radiative transitions are shown by arrows. The absorption spectra were recorded in the 3000–39000 cm^{-1} spectral region with a Perkin-Elmer Lambda-9 spectrophotometer. The fluorescence spectra were recorded using setup on the basis of a DFS-32 spectrometer with removable diffraction gratings.

The experimental oscillator strengths $f_{i,j}$ and integrated cross-sections $\sigma_{i,j}$ of the transitions from the ground state i to the excited multiplets j have been determined from the absorption spectra in accordance with the expression

$$f_{i,j}^{\mathrm{exp}} = \frac{mc^2}{N\pi e^2} \int K_{i,j}(\nu)\mathrm{d}\nu = \frac{mc^2}{\pi e^2}\sigma_{i,j}, \tag{2.2}$$

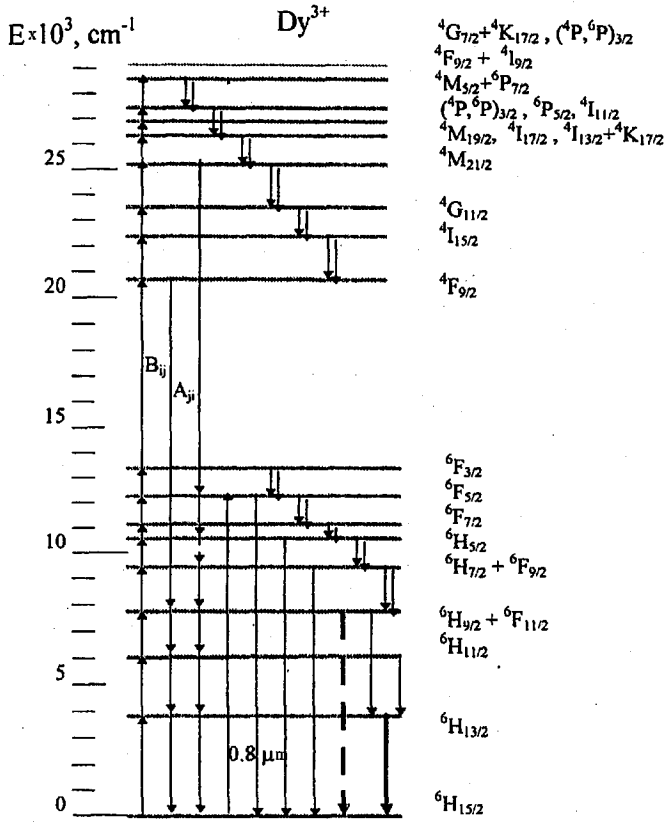

Fig. 1. Diagram of energy levels and transitions between them for dysprosium ion in YLF:Dy^{3+} and KPb_2Cl_5:Dy^{3+}. Ground state absorption (B_{ij}) and emission (A_{ji}) are designated by thin arrows, double arrows are non-radiative transitions, thick dash arrow indicates the transition in KPb_2Cl_5:Dy^{3+} responsible for amplification of a small signal at 1.3 μm, and thick solid arrow shows 3 μm probable laser transition in Dy^{3+} doped studied crystals.

where m and e are the mass and the charge of an electron, c is the velocity of light, $\int K_{i,j}(\nu)\mathrm{d}\nu$ is the integrated absorption coefficient corresponding to the transition $i \rightarrow j$, and N is the concentration of active ions.

The oscillator strengths $f_{i,j}^{\mathrm{exp}}$ for transitions from the ground state $^6H_{15/2}$ to the excited states of Dy^{3+} ions in YLF:Dy^{3+} and KPb_2Cl_5:Dy^{3+} crystals are given in Tables I and II.

The following expression was taken for the integrated cross-section $\sigma_{i,j}$:

$$\sigma_{i,j} = \int \sigma_{i,j}(\nu)\mathrm{d}\nu = \frac{1}{N}\int k_{i,j}(\nu)\mathrm{d}\nu, \tag{2.3}$$

where $\sigma_{i,j}(\nu) = k_{i,j}(\nu)/N$ is the cross-section at the frequency ν in cm^2. For the frequency in the line maximum $\sigma_{i,j}^{\mathrm{p}} = \sigma_{i,j}(\nu_{\max})$ it is the so-called peak cross-section.

Figures 2a and b show the absorption cross-section spectra in the 3300–20000 cm^{-1} spectral region (transitions from $^6H_{15/2}$ to $^6H'_J$, ^6F_J levels, see Fig. 1)

TABLE I

Experimental f_{exp} and calculated f_{calc} oscillator strengths of dipole–dipole $i \rightarrow j$ transitions in YLF:Dy^{3+} crystals.

Transition from $^6H_{15/2}$ to:	$\overline{\nu}$ [cm^{-1}]	$f_{exp} \times 10^6$	$f_{calc} \times 10^6$
$^6H_{13/2}$	3400	1.05	0.85
$^6H_{11/2}$	5875	0.87	0.99
$^6H_{9/2} + {}^6F_{11/2}$	7732	2.71	2.81
$^6H_{7/2} + {}^6F_{9/2}$	9155	2.03	2.15
$^6H_{5/2}$	10200	0.18	0.01
$^6F_{7/2}$	10900	1.72	1.96
$^6F_{5/2}$	12338	1.17	1.06
$^6F_{3/2} + {}^6F_{1/2}$	13337	0.24	0.21

TABLE II

Experimental f_{exp} and calculated f_{calc} oscillator strengths of dipole–dipole $i \rightarrow j$ transitions in KPb_2Cl_5:Dy^{3+} crystals.

Transition from $^6H_{15/2}$ to:	$\overline{\nu}$ [cm^{-1}]	$f_{exp} \times 10^6$	$f_{calc} \times 10^6$
$^6H_{13/2}$	3472	3.52	3.36
$^6H_{11/2}$	5765	2.25	2.43
$^6H_{9/2} + {}^6F_{11/2}$	7711	20.07	20.15
$^6H_{7/2} + {}^6F_{9/2}$	8995	4.31	4.43
$^6H_{5/2}$	10291	0.01	0.01
$^6F_{7/2}$	10978	3.36	3.43
$^6F_{5/2}$	12254	1.90	1.70
$^6F_{3/2} + {}^6F_{1/2}$	13110	0.32	0.32

for YLF:Dy^{3+} and KPb_2Cl_5:Dy^{3+} crystals, respectively. The maximal peak absorption cross-sections $\sigma^p_{i,j}(\lambda) = k_{i,j}(\lambda)/N_{Dy}$ for the most intense absorption bands of studied crystals are listed in Table III.

Parameters of spontaneous radiative transitions were found by the Judd–Ofelt method [4, 5]. The oscillator strength of the electric dipole transition $i \rightarrow j$, within the $4f^n$ configuration of the rare-earth ions in the crystal can be represented as the sum

$$f^{calc}_{ij}([S'L']J', [SL]J) = \frac{8\pi^2 mc\nu\chi}{3h(2J+1)n^2} \sum_t \Omega_t |\langle |SL|J||U^{(t)}||S'L'|J'\rangle|^2, \quad (2.4)$$

where $\langle |SL|J||U^{(t)}||S'L'|J'\rangle$ are the matrix elements of unit tensor operator, $\chi = n(n^2+2)^2/9$ for the dipole transition. The experimental oscillator strengths for the electric dipole transitions were calculated from the relation $f^{ed} = f^{exp} - f^{md}$. The oscillator strengths of magnetic dipole transitions f^{md} were taken from [6]. By equating experimental and calculated oscillator strengths, $f^{calc}_{ij} = f^{exp}_{ij}$ and solving

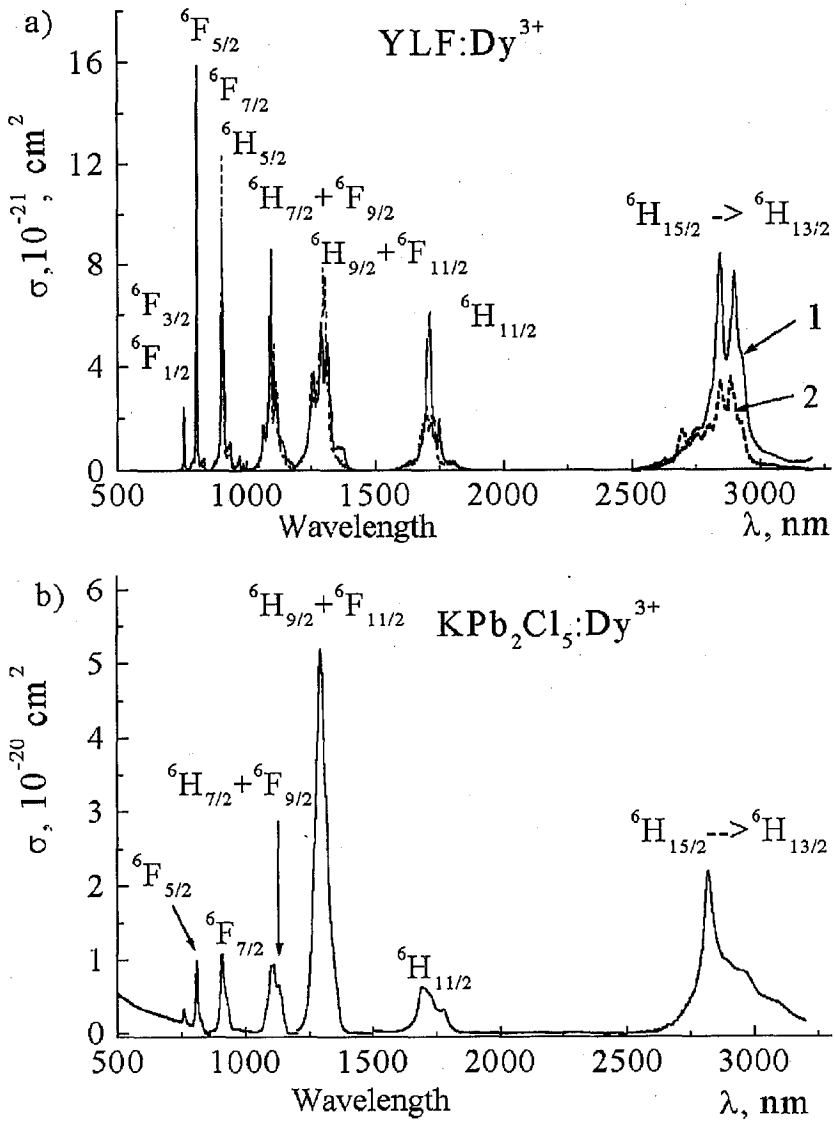

Fig. 2. Absorption cross-section spectra at 300 K: (a) polarized spectra of YLF:Dy^{3+} crystal for $\pi + \sigma$ polarization (solid curve 1) and σ polarization (dash curve 2), (b) non-polarized spectrum of absorption cross-section for KPb_2Cl_5:Dy^{3+} crystal.

the system of Eqs. (2.4) for the intensity parameters Ω_t by the least squares method, we can find the values of Ω_t. These parameters are

$$\Omega_2 = 2.4\times10^{-20},\ \Omega_4 = 1.07\times10^{-20},\ \Omega_6 = 2.9\times10^{-20}\ \text{cm}^2 \text{ for YLF}:\text{Dy}^{3+},$$

and

$$\Omega_2 = 23\times10^{-20},\ \Omega_4 = 3.3\times10^{-20},\ \Omega_6 = 3.9\times10^{-20}\ \text{cm}^2 \text{ for } KPb_2Cl_5:\text{Dy}.$$

TABLE III

Absorption cross-section for YLF:Dy^{3+} and KPb_2Cl_5:Dy^{3+}.

$i \rightarrow j$ transition	$LiYF_4$:Dy^{3+}		KPb_2Cl_5:Dy^{3+}	
	λ [nm]	$\sigma^p \times 10^{20}$ [cm^2]	λ [nm]	$\sigma^p \times 10^{20}$ [cm^2]
$^6H_{15/2} \rightarrow {}^4M_{5/2} + {}^6P_{7/2}$	350	1.12 ($\pi + \sigma$)	352.6	2.4
$^6H_{15/2} \rightarrow {}^6F_{5/2}$	805.4	1.03 ($\pi + \sigma$)	810.4	0.9
$^6H_{15/2} \rightarrow {}^6H_{7/2} + {}^6F_{9/2}$	1297	0.78 (σ)	1297	5.18
$^6H_{15/2} \rightarrow {}^6H_{13/2}$	2843	0.84 ($\pi + \sigma$)	2820	2.19

The theoretical oscillator strengths for the absorption bands f_{ij}^{calc} were calculated with these parameters for YLF:Dy^{3+} and KPb_2Cl_5:Dy^{3+} crystals; they are listed in Tables I and II. Good agreement between the experimental and calculated oscillator strengths of the transitions from the ground state $^6H_{15/2}$ to the excited states in studied crystals permitted us to calculate the characteristics of radiative transitions with these intensity parameters Ω_t.

The following well-known expressions were used to determine the values of the oscillator strengths $f_{j,i}$, the probabilities $A_{j,i}^{\mathrm{T}}$, and branching ratios $\beta_{j,i}^{\mathrm{T}}$ of the radiative transitions $j \rightarrow i$:

$$f_{j,i}^{\mathrm{calc}} = \frac{g_i}{g_j} f_{i,j}^{\mathrm{calc}}, \tag{2.5}$$

$$A_{ji}^{\mathrm{T}}([S'L']J', [SL]J) = \frac{8\pi^2 e^2 \nu_{ji}^2 n^2}{mc} \frac{(2J_i + 1)}{(2J_j + 1)} f_{ij}^{\mathrm{calc}}([S'L']J', [SL]J), \tag{2.6}$$

$$\beta_{j,i}^{\mathrm{T}} = \frac{A_{j,i}^{\mathrm{T}}}{\sum_k A_{j,k}^{\mathrm{T}}}. \tag{2.7}$$

Here ν is the average transition frequency in cm^{-1}, $g_{i(j)}$ is the degeneracy of the i (j) level, and n is the refractive index at the frequency ν.

The radiative lifetimes were found from the total probabilities of radiative transitions from the level j:

$$\tau_{j,0} = \left(\sum_k A_{jk} \right)^{-1}, \tag{2.8}$$

and the non-radiative transition probability W_j can be estimated from the intrinsic level lifetime τ_j:

$$(\tau_j)^{-1} = (\tau_{j,0})^{-1} + W_j. \tag{2.9}$$

The calculated oscillator strengths, radiative probabilities, and branching ratios for radiative transitions between sextet Dy^{3+} levels in YLF:Dy^{3+} and KPb_2Cl_5:Dy^{3+} crystals are given in Tables IV and V, respectively.

To estimate the luminescence intensity, certain information about non-radiative transition rates is required.

Luminescence quantum yield from the excited levels is

$$\eta = \sum_j A_{ij} / (\sum_j A_{ij} + W_{ij}^{\mathrm{NR}}) \tag{2.10}$$

TABLE IV

The calculated oscillator strengths f_{calc}, radiative probabilities A_{ji}, branching ratios β_{ji}, radiative lifetimes τ_0, and multiphonon non-radiative transition rates W^{NR} for dipole–dipole ($j \rightarrow i$) transitions in YLF:Dy^{3+} crystals.

Transition $j \rightarrow i$	$\bar{\nu}$ [cm^{-1}]	f_{calc} $\times 10^6$	A_{ji} [s^{-1}]	β_{ji}	τ_0 [ms]	W^{NR} [s^{-1}]
$^6H_{13/2} \rightarrow {}^6H_{15/2}$	3400	0.97	16	1	62.5	300
$^6H_{11/2} \rightarrow {}^6H_{13/2}$	2475	0.34	2.9	0.044	14.8	9000
$\rightarrow {}^6H_{15/2}$	5875	1.32	64.7	0.956		
$^6H_{9/2} + {}^6F_{11/2} \rightarrow {}^6H_{11/2}$	1900	0.42	2.2	0.011	5.2	6×10^4
$\rightarrow {}^6H_{13/2}$	4150	1.18	29	1.15		
$\rightarrow {}^6H_{15/2}$	7550	2.0	162	0.839		
$^6H_{7/2} + {}^6F_{9/2} \rightarrow {}^6H_{9/2} + {}^6F_{11/2}$	1350	0.25	0.65	0.002	3.5	5×10^5
$\rightarrow {}^6H_{11/2}$	3250	0.54	8.06	0.03		
$\rightarrow {}^6H_{13/2}$	5500	1.47	63.5	0.23		
$\rightarrow {}^6H_{15/2}$	8900	1.86	210	0.74		
$^6H_{5/2} \rightarrow {}^6H_{7/2} + {}^6F_{9/2}$	1100	0.48	0.83	0.017	20.2	10^6
$\rightarrow {}^6H_{9/2} + {}^6F_{11/2}$	2450	0.64	5.5	0.11		
$\rightarrow {}^6H_{11/2}$	4350	0.86	23	0.47		
$\rightarrow {}^6H_{13/2}$	6600	0.27	17	0.34		
$\rightarrow {}^6H_{15/2}$	10100	0.022	3.2	0.064		
$^6F_{7/2} \rightarrow {}^6H_{5/2}$	800	0.18	0.16	0.0002	1.3	4×10^6
$\rightarrow {}^6H_{7/2} + {}^6F_{9/2}$	1900	0.22	1.11	0.0015		
$\rightarrow {}^6H_{9/2} + {}^6F_{11/2}$	3250	0.98	14.7	0.02		
$\rightarrow {}^6H_{11/2}$	5100	1.6	60.5	0.08		
$\rightarrow {}^6H_{13/2}$	7400	0.57	44.8	0.06		
$\rightarrow {}^6H_{15/2}$	10800	3.9	644	0.84		
$^6F_{5/2} \rightarrow {}^6F_{7/2}$	1400	0.04	0.11	0.0001	1.0	4×10^5
$\rightarrow {}^6H_{5/2}$	2200	0.19	1.3	0.001		
$\rightarrow {}^6H_{7/2} + {}^6F_{9/2}$	3300	1.4	22	0.023		
$\rightarrow {}^6H_{9/2} + {}^6F_{11/2}$	4650	1.4	44	0.046		
$\rightarrow {}^6H_{11/2}$	6550	1.1	65	0.068		
$\rightarrow {}^6H_{13/2}$	8800	2.1	230	0.24		
$\rightarrow {}^6H_{15/2}$	12200	2.8	590	0.62		
$^6F_{3/2} \rightarrow {}^6F_{5/2}$	800	0.023	0.021	0.0000	1.18	4×10^6
$\rightarrow {}^6F_{7/2}$	2200	0.033	0.23	0.0002		
$\rightarrow {}^6H_{5/2}$	3000	0.48	6.1	0.007		
$\rightarrow {}^6H_{7/2} + {}^6F_{9/2}$	4100	0.66	15.7	0.018		
$\rightarrow {}^6H_{9/2} + {}^6F_{11/2}$	5450	2.3	97	0.11		
$\rightarrow {}^6H_{11/2}$	7300	0.76	58	0.07		
$\rightarrow {}^6H_{13/2}$	9600	3.7	480	0.57		
$\rightarrow {}^6H_{15/2}$	13000	0.8	190	0.23		
$^6F_{1/2} \rightarrow {}^6F_{3/2}$	400	0.01	0.002	0.0000	1.3	2×10^7
$\rightarrow {}^6F_{5/2}$	1200	0.02	0.047	0.0000		
$\rightarrow {}^6F_{7/2}$	2500	0.05	0.49	0.0006		
$\rightarrow {}^6H_{5/2}$	3400	1.1	18	0.024		
$\rightarrow {}^6H_{7/2} + {}^6F_{9/2}$	4500	0.47	14	0.018		
$\rightarrow {}^6H_{9/2} + {}^6F_{11/2}$	5850	0.7	34	0.045		
$\rightarrow {}^6H_{11/2}$	7700	5.2	442	0.58		
$\rightarrow {}^6H_{13/2}$	10000	2.0	288	0.38		
$\rightarrow {}^6H_{15/2}$	13400	0	0	0.000		

TABLE V

The calculated oscillator strengths $f_{\rm calc}$, radiative probabilities A_{ji}, branching ratios β_{ji}, radiative lifetimes τ_0, and multiphonon non-radiative transition rates $W^{\rm NR}$ for dipole–dipole ($j \to i$) transitions in $KPb_2Cl_5:Dy^{3+}$ crystals.

Transition $j \to i$	$\bar{\nu}$ [cm^{-1}]	$f_{\rm calc}$ $\times 10^6$	A_{ji} [s^{-1}]	β_{ji}	τ_0 [ms]	$W^{\rm NR}$ [s^{-1}]
$^6H_{13/2} \to {}^6H_{15/2}$	3400	3.76	84	1	11.9	0
$^6H_{11/2} \to {}^6H_{13/2}$	2475	2.56	30	0.12	4.0	< 1
$\to {}^6H_{15/2}$	5875	3.30	220	0.88		
$^6H_{9/2} + {}^6F_{11/2} \to {}^6H_{11/2}$	1900	1.75	12	0.007	0.581	≈ 1
$\to {}^6H_{13/2}$	4150	3.89	129	0.075		
$\to {}^6H_{15/2}$	7550	14.34	1580	0.918		
$^6H_{7/2} + {}^6F_{9/2} \to {}^6H_{9/2} + {}^6F_{11/2}$	1350	1.41	5	0.004	0.85	$\approx 10^3$
$\to {}^6H_{11/2}$	3250	2.81	57	0.048		
$\to {}^6H_{13/2}$	5500	8.84	517	0.440		
$\to {}^6H_{15/2}$	8900	3.90	597	0.508		
$^6H_{5/2} \to {}^6H_{7/2} + {}^6F_{9/2}$	1100	2.16	5	0.042	8.4	$\approx 10^4$
$\to {}^6H_{9/2} + {}^6F_{11/2}$	2450	1.52	18	0.151		
$\to {}^6H_{11/2}$	4350	1.43	52	0.437		
$\to {}^6H_{13/2}$	6600	0.43	37	0.310		
$\to {}^6H_{15/2}$	10100	0.04	7	0.059		
$^6F_{7/2} \to {}^6H_{5/2}$	800	0.34	0.4	0.0002	0.41	$\approx 10^7$
$\to {}^6H_{7/2} + {}^6F_{9/2}$	1900	1.27	9	0.004		
$\to {}^6H_{9/2} + {}^6F_{11/2}$	3250	5.24	107	0.044		
$\to {}^6H_{11/2}$	5100	11.4	575	0.235		
$\to {}^6H_{13/2}$	7400	2.17	230	0.094		
$\to {}^6H_{15/2}$	10800	6.75	1521	0.623		
$^6F_{5/2} \to {}^6F_{7/2}$	1400	0.38	1.5	0.001	0.36	$\approx 10^5$
$\to {}^6H_{5/2}$	2200	1.07	10	0.004		
$\to {}^6H_{7/2} + {}^6F_{9/2}$	3300	6.23	132	0.048		
$\to {}^6H_{9/2} + {}^6F_{11/2}$	4650	11.4	476	0.172		
$\to {}^6H_{11/2}$	6550	2.42	200	0.072		
$\to {}^6H_{13/2}$	8800	4.30	644	0.233		
$\to {}^6H_{15/2}$	12200	4.51	1297	0.470		
$^6F_{3/2} \to {}^6F_{5/2}$	800	0.21	0.3	0.000	0.46	$\approx 10^8$
$\to {}^6F_{7/2}$	2200	0.34	3	0.001		
$\to {}^6H_{5/2}$	3000	4.43	77	0.036		
$\to {}^6H_{7/2} + {}^6F_{9/2}$	4100	3.57	116	0.054		
$\to {}^6H_{9/2} + {}^6F_{11/2}$	5450	4.30	247	0.114		
$\to {}^6H_{11/2}$	7300	2.32	239	0.111		
$\to {}^6H_{13/2}$	9600	5.94	1057	0.489		
$\to {}^6H_{15/2}$	13000	1.29	421	0.195		
$^6F_{1/2} \to {}^6F_{3/2}$	400	0.12	0.04	0.000	0.47	$\approx 10^9$
$\to {}^6F_{5/2}$	1200	0.27	0.74	0.000		
$\to {}^6F_{7/2}$	2500	0.19	2.50	0.001		
$\to {}^6H_{5/2}$	3400	12.7	284	0.134		
$\to {}^6H_{7/2} + {}^6F_{9/2}$	4500	1.79	70	0.033		
$\to {}^6H_{9/2} + {}^6F_{11/2}$	5850	2.51	166	0.079		
$\to {}^6H_{11/2}$	7700	8.42	964	0.456		
$\to {}^6H_{13/2}$	10000	3.25	627	0.297		
$\to {}^6H_{15/2}$	13400	0	0	0.000		

and strongly depends from the non-radiative relaxation rates W_{ij}^{NR} for a small energy gap between the energy levels ΔE_{ij}. It was found by Miyakawa and Dexter [7] that multiphonon non-radiative transition rate (in a single frequency approach) depended exponentially on the energy gap ΔE_{ij}:

$$W_{ij}^{\mathrm{NR}}(\Delta E_{ij}) = W_{ij}(0)\exp(-\beta \Delta E_{ij}), \tag{2.11}$$

where $W_{ij}(0)$ is the relaxation rate at $T = 0$, and

$$\beta = (1/\hbar\omega_0)\left\{\ln\left[(p/a)\left(\overline{n}(\omega_0)+1\right)\right]-1\right\}. \tag{2.12}$$

Here $\hbar\omega_0$ is the phonon energy which is equal or less than the limiting phonon energy of the crystal, p is the number of phonons emitted into crystal-matrix, a is the electron–phonon coupling constant, $\overline{n}(\omega_0)$ is the mean equilibrium value for the phonon number with the energy $\hbar\omega_0$:

$$\overline{n}_i(\omega_0) = [\exp(\hbar\omega_0/kT)-1]^{-1}. \tag{2.13}$$

Assuming a weak electron–phonon coupling and low value of $\overline{n}(\omega_0)$, the dependence $W_{ij}^{\mathrm{NR}}(\Delta E_{ij})$ could be approximated as the exponential one (2.11). This expression coincides with the phenomenological formula

$$W_{ij}^{\mathrm{NR}}(\Delta E_{ij}) = B\exp(-\alpha E_0), \tag{2.14}$$

commonly used for estimating the multiphonon non-radiative transition rates in a given crystal [8, 9]. This expression was explained by Riseberg and Moos [10].

The results of calculation of the multiphonon non-radiative transition rates in YLF and KPb_2Cl_5 crystals within the framework of both mentioned models are

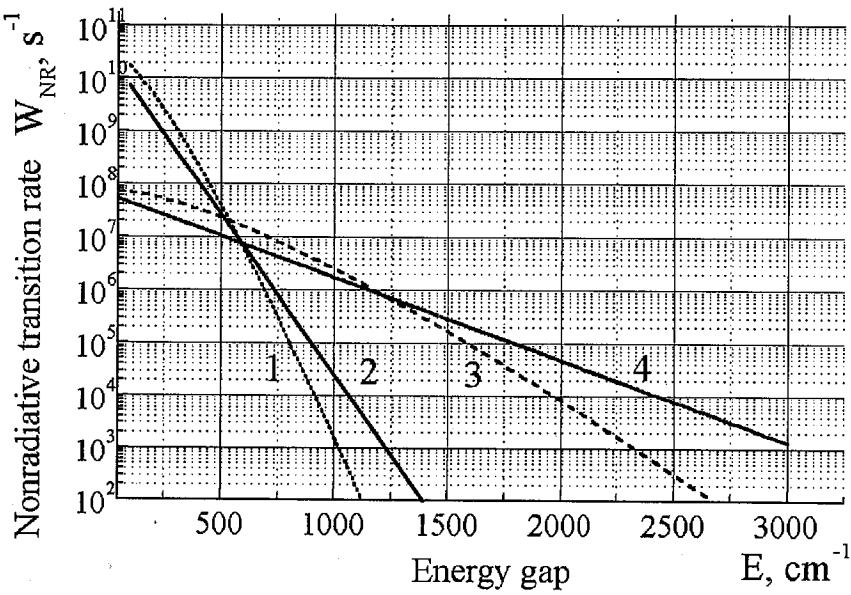

Fig. 3. Calculated dependence of non-radiative transition rates for KPb_2Cl_5 (1, 2) and YLF (3, 4) crystal-matrices. 1, 3 — Miyakawa and Dexter model, 2, 4 — Riseberg and Moos model.

represented in Fig. 3. For YLF crystals we used $\hbar\omega_0 \approx 560$ cm^{-1} [11], parameters $B = 6.7 \times 10^7$ s^{-1}, $\alpha = 3.6 \times 10^{-3}$ cm [12], and $a = 0.1$. For chlorides the typical values are: $B = 1.5 \times 10^{10}$ s^{-1}, $\alpha = 1.3 \times 10^{-2}$ cm and $a = 0.04$ [13]. The value of $\hbar\omega_0 = 200$ cm^{-1} for KPb_2Cl_5 was found from Raman spectrum. The dependence $W1(e) = W_{ij}^{NR}1(\Delta E_{ij})$ was calculated using formulas (2.11)–(2.13) and $W2(E) = W_{ij}^{NR}2(\Delta E_{ij})$ by formula (2.14). The results of estimating the non-radiative transition rates W_{ij}^{NR} in YLF:Dy^{3+} and KPb_2Cl_5:Dy^{3+} with the

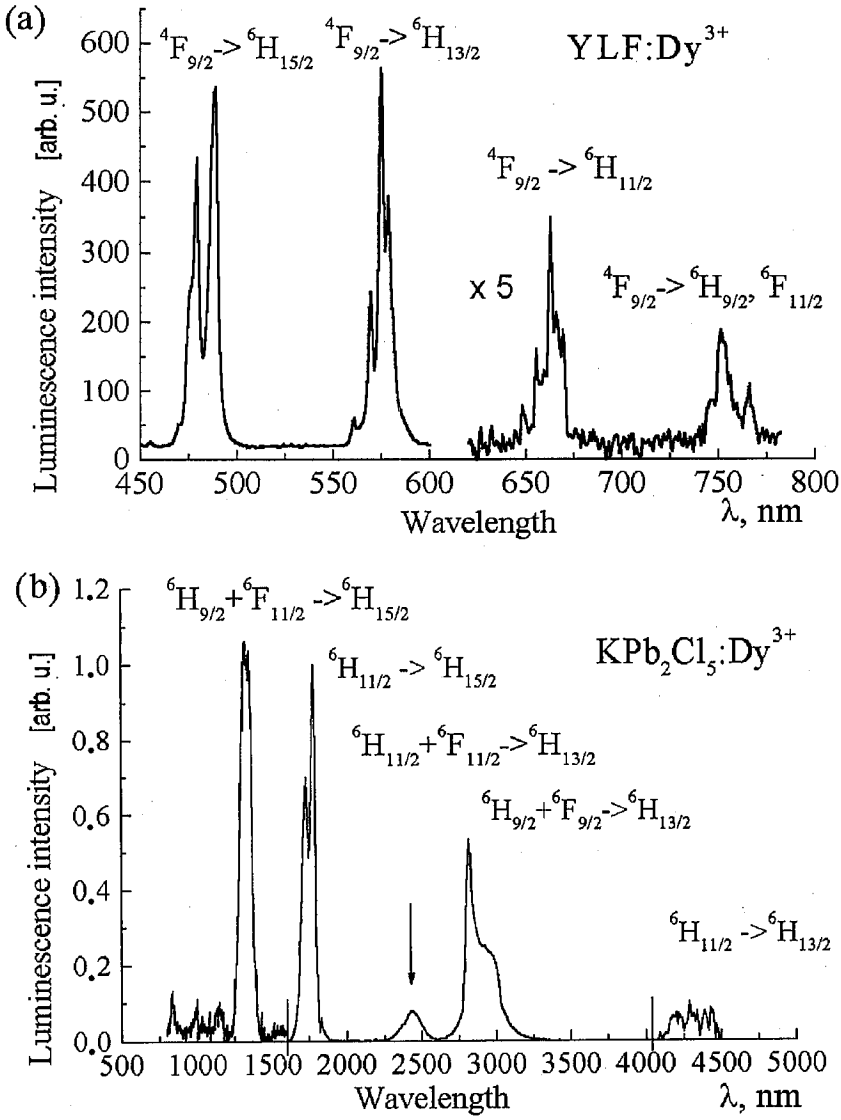

Fig. 4. Luminescence spectra of YLF:Dy^{3+} (a) and KPb_2Cl_5:Dy^{3+}(b) at $T = 300$ K.

use of empirical dependence (2.14) are shown in Tables IV and V. As a matter of fact, the luminescent properties of crystals depend on the relation between radiative and non-radiative probabilities for each of excited levels. From Fig. 3, one can conclude that in YLF:Dy^{3+} all excited levels separated by the energy gap $\Delta E_{ij} < 2000$ cm^{-1} are quenched. In KPb_2Cl_5:Dy^{3+} almost all excited dysprosium levels are radiative, considerable quenching ($W_{ij}^{NR} > 10^3$ s^{-1}) can be observed for the excited levels separated by the energy gap $\Delta E_{ij} < 1000$ cm^{-1}. These conclusions are in good agreement with the results of examination of luminescence spectra of studied crystals shown in Fig. 4.

If YLF:Dy^{3+} crystal was excited by Xe-lamp through UV filter (340–400 nm), the luminescence was observed only from the $^4F_{9/2}$ level. The luminescence bands (Fig. 4a) were assigned to the transitions $^4F_{9/2} \rightarrow {}^4F_{11/2}, {}^6H_J$ (Fig. 1). Under UV excitation of KPb_2Cl_5:Dy^{3+} crystals, one can see luminescence in the spectral region 410–850 nm corresponding to transitions from $^4F_{9/2}$, $^4I_{15/2}$ and $^4M_{21/2}$ levels. With IR excitation no luminescence was observed in YLF:Dy^{3+} except that at 3 μm corresponding to the $^6H_{13/2} \rightarrow {}^6H_{15/2}$ transition, and under the same excitation conditions in KPb_2Cl_5:Dy^{3+} we observed luminescence at 1.3 μm, 1.7 μm, 2.4 μm, 2.9 μm, and 4.3 μm (Fig. 4b). The luminescence lifetime Dy^{3+} for transition at 1.3 μm $^6H_{9/2} + {}^6F_{11/2} \rightarrow {}^6H_{15/2}$ was measured using a short-pulse IR pumping. Luminescence decay was exponential with the $\tau_{exp} = 653$ μs in KPb_2Cl_5:Dy^{3+} (1 mol.%).

3. Discussion

Comparison of the Dy^{3+} absorption and emission spectra in YLF and KPb_2Cl_5 matrices showed that, in accordance with the crystalline structure, the YLF:Dy^{3+} crystals have narrow polarized lines but KPb_2Cl_5:Dy^{3+} spectra exhibit non-structured absorption bands typical of disordered structure (Figs. 2a, 2b, 4a, 4b). It is remarkable that the most intense absorption band ($\sigma^p(\lambda) = 5.18 \times 10^{-20}$ cm^2) in KPb_2Cl_5:Dy^{3+} corresponds to $^6H_{15/2} \rightarrow {}^6H_{9/2} + {}^6F_{11/2}$ transition ($\lambda = 1297$ nm), this transition is the most favorable for application in telecommunication amplifiers. Moreover, absorption bands near 800 nm corresponding to the $^6H_{15/2} \rightarrow {}^6F_{5/2}$ transition can be used for LD pumping of Dy^{3+}-doped crystals. These intense bands have the peak absorption cross-sections $\sigma^p(\lambda) = 1.03 \times 10^{-20}$ cm^2 for the nonpolarized absorption band near 805 nm in YLF:Dy^{3+}, and $\sigma^p(\lambda) = 0.9 \times 10^{-20}$ cm^2 for the absorption band near 810 nm in KPb_2Cl_5:Dy^{3+} (Table III), their spectral positions coincide with the laser diode emission spectrum. Other IR absorption bands corresponding to the transitions $^6H_{15/2} \rightarrow {}^6H_{13/2}$, $^6H_{15/2} \rightarrow {}^6H_{9/2} + {}^6F_{11/2}$, $^6H_{15/2} \rightarrow {}^6H_{7/2} + {}^6F_{9/2}$, and $^6H_{15/2} \rightarrow {}^6F_{7/2}$ have high intensity but none of them matches the LD pumping.

From the luminescence spectra of YLF:Dy^{3+} under UV excitation (Fig. 4a) it follows that all groups of lines correspond to transitions from one level $^4F_{9/2}$ on ^6F_J and ^6H_J levels. Considering the rates of multiphonon relaxation in YLF:Dy^{3+} (Fig. 3, and data in Table IV) the conclusion can be made that under UV excitation the radiative transitions from $^4F_{9/2}$ level occur in YLF:Dy^{3+}, while at IR excitation the only radiative transition $^6H_{13/2} \rightarrow {}^6H_{15/2}$ at 3 μm is possible. This transition is the most efficient luminescent transition of YLF:Dy^{3+} crystals under LD pump

because luminescence efficiency for all other IR transitions are very low due to high non-radiative probabilities for ^6F_J and ^6H_J levels excepting the $^6H_{13/2}$ level. Therefore, according to the calculated estimates the transition $^6H_{13/2} \rightarrow {}^6H_{15/2}$ may be considered as the laser one at 3 μm range.

On the contrary, in KPb_2Cl_5:Dy^{3+} crystals several quartet levels and almost all sextet levels are initial levels of radiative transitions that is why luminescence spectra of Dy^{3+} ions have a lot of bands not only in UV, VIS, and 3 mm spectral regions, as in fluoride crystals, but also in IR — up to 4 mm (Fig. 1). Experimental luminescence spectra of KPb_2Cl_5:Dy^{3+} crystals (Fig. 4b) are in good agreement with the calculated estimates: luminescence in KPb_2Cl_5:Dy^{3+} was really observed at 1.3 μm ($^6H_{9/2} + {}^6F_{11/2} \rightarrow {}^6H_{15/2}$); 1.7 μm ($^6H_{11/2} \rightarrow {}^6H_{15/2}$); 2.4 μm ($^6H_{9/2} + {}^6F_{11/2} \rightarrow {}^6H_{13/2}$); 2.9 μm ($^6H_{13/2} \rightarrow {}^6H_{15/2}$) and 4.3 μm ($^6H_{11/2} \rightarrow {}^6H_{15/2}$). The luminescence lifetime of Dy^{3+} ions was measured for transition at 1.3 μm ($^6H_{9/2} + {}^6F_{11/2} \rightarrow {}^6H_{15/2}$). Luminescence decay is exponential with $\tau_{exp} = 653$ μs in KPb_2Cl_5:Dy^{3+} (1 mol.%). This value was longer than calculated radiative lifetime $\tau_0 = 581$ μs shown in Table V. It may be partly explained by the effect of reabsorption for the resonant transition with a high oscillator strength.

Preliminary results of experimental study of small signal gain measurements were made on KPb_2Cl_5:Dy^{3+} crystal with a Cr:LiSAF laser providing 0.2 ms pump pulses at 910 nm, and a CW Nd^{3+}:YAG laser probe beam at 1319 nm line. With the available pump energy density $F = 175$ J/cm^2 the probe signal increases by 12% above the ground state absorption. These data show new possibilities for development of the 1.3 μm optical amplifier with a high quantum efficiency based on Dy^{3+}-doped double chlorides.

4. Conclusions

We have studied spectroscopic properties of Dy^{3+}-doped double lithium-yttrium fluoride and double potassium-lead chloride crystals. The KPb_2Cl_5 crystals have monoclinic structure with non-equivalent sites of cations (Pb^{2+} and K^+) for replacement by Dy^{3+}. We obtained the effective distribution coefficients $K_{Dy} = 1$ for KPb_2Cl_5:Dy^{3+} and $K_{Dy} = 0.95$ for YLF:Dy^{3+}. The optical spectra (absorption cross-sections, luminescence spectra, and Raman spectra) of chloride crystals were typical of disordered structure of impurity centers. Dysprosium ions substitute different non-equivalent cation sites, the charge compensation with forming the cation vacancy is required in Dy^{3+} doped chloride crystals.

The oscillator strengths of transitions from the ground state have been determined and the intensity parameters have been obtained using Judd–Ofelt method. The probabilities of radiative and non-radiative Dy^{3+} transitions were estimated in both systems. IR luminescence spectra show intense bands near 1.3 and 2.9 μm in KPb_2Cl_5:Dy^{3+} and the only one band at 2.9 μm in YLF:Dy^{3+} in accordance with the calculated estimates.

On the basis of calculated and experimental data some conclusions were made about possible practical applications of studied crystals:

— the YLF:Dy^{3+} crystals may be considered as promising active media for 3 μm lasers;

— narrow phonon spectrum of double chloride crystals caused a lot of IR radiative transitions in dysprosium, some of them having a long lifetime and high intensity, could be considered as the highly probable lasing transitions, so KPb_2Cl_5:Dy crystals are promising active media for laser action at a number of wavelengths up to 4 μm;

— high luminescence intensity of the KPb_2Cl_5:Dy crystals at 1.3 μm and long lifetime (0.67 ms) of the initial level of this transition, together with gain effect at 1.319 μm make us conclude that these crystals will be perspective for application in telecommunication amplifiers.

Acknowledgments

The work was partly supported by CRDF, grant No. 1355 (129100) and by RFBR grant No. 97-02-16439.

References

[1] L.F. Johnson, H.J. Guggenheim, *Appl. Phys. Lett.* **23**, 96 (1973).

[2] B.M. Antipenko, A.L. Ashkalunin, A.A. Mak, B.V. Sinitsyn, Yu.V. Tomashevich, G.S. Shahkalamyan, *Kvantovaya Elektron. (USSR)* **7**, 983 (1980).

[3] A.M. Tkachuk, A.V. Poletimova, M.A. Petrova, V.Ju. Egorov, N.E. Korolev, *Opt. Spektrosk.* **70**, 1230 (1991).

[4] B.R. Judd, *Phys. Rev.* **127**, 750 (1963).

[5] G.S. Ofelt, *J. Chem. Phys.* **37**, 511 (1962).

[6] W.T. Carnall, B.H. Matsinger, V. Donlan, G.T. Surratt, *J. Chem. Phys.* **49**, 4412 (1972).

[7] T. Miyakava, D.L. Dexter, *Phys. Rev. B* **1**, 2961 (1970).

[8] M.J. Weber, *Phys. Rev.* **171**, 283 (1968).

[9] M.J. Weber, *Phys. Rev.* **157**, 262 (1967).

[10] L.A. Riseberg, H.W. Moos, *Phys. Rev.* **174**, 429 (1968).

[11] H.H. Caspers, H.E. Rast, *J. Lumin.* **10**, 347 (1975).

[12] A.M. Tkachuk, A.V. Chilko, M.V. Petov, *Opt. Spektrosk.* **58**, 361 (1985).

[13] L.A. Riseberg, M.J. Weber, *Prog. Opt.* **14**, 91 (1977).